Continuum Mech. Thermodyn.
https://doi.org/10.1007/s00161-022-01179-4

ORIGINAL ARTICLE

Yiming Liu · Bilen Emek Abali · Hua Yang · Wolfgang H. Müller

Plate capacitor problem as a benchmark case for verifying the finite element implementation

Received: 26 August 2022 / Accepted: 9 December 2022
© The Author(s) 2022

Abstract In this work, parallel plate capacitors are numerically simulated by solving weak forms within the framework of the finite element method. Two different domains are studied. We study the infinite parallel plate capacitor problem and verify the implementation by deriving analytical solutions with a single layer and multiple layers between two plates. Furthermore, we study the finite parallel plate capacitor problem and verify it by Love's potential equation and Xiang's capacitance equation. Moreover, the fringing effect is considered and extended to problems with multiple dielectric layers, such a solution is not possible by means of the existing analytical solutions. Besides, we realize the possibility of choosing different boundary conditions (electric potential boundary conditions and charge density boundary conditions) by changing the weak form. Finally, a transient solution that includes dielectric loss and calculates the quality factor of a capacitor is presented, which may be used in capacitor design. Convergence and consistency of results are demonstrated by comparing the results between analytical and numerical solutions and also the results from different boundary conditions.

Keywords Analytical solution · Dielectrics · Capacitor · Finite element method · FEniCS

1 Introduction

Capacitors and transistors are the main electronic components shaping the future. On a modern tablet or laptop, it is standard to have a 4 GB DRAM composed of 32 billion capacitors. Trench or stacked capacitors are built in layers or etched in silicon. The size of such a capacitor is in nanometer. Technically two parallel coaxial plates and an insulator compose a capacitor. This "important" electronic component has a long and rich history in electrostatics. An expression for the electric potential is given in [1] for a parallel plate capacitor as an infinite series of spheroidal harmonics with coefficients satisfying an infinite set of linear equations. Based on this idea, this series is reduced to the Laplace problem in [2,3] that indeed has a solution as a linear integral

Communicated by Andreas Öchsner.

H. Yang (✉)
School of Mechanical Engineering, Hebei University of Technology, Tianjin 300401, China
E-mail: hua.yang@hebut.edu.cn

B. E. Abali (✉)
Institute of Mechanics, Technische Universität Berlin, Einsteinufer 5, 10587 Berlin, Germany
E-mail: bilenemek@abali.org

Y. Liu · W. H. Müller
Division of Applied Mechanics, Department of Materials Science and Engineering, Uppsala University, Box 534, 751 21 Uppsala, Sweden

Published online: 23 December 2022

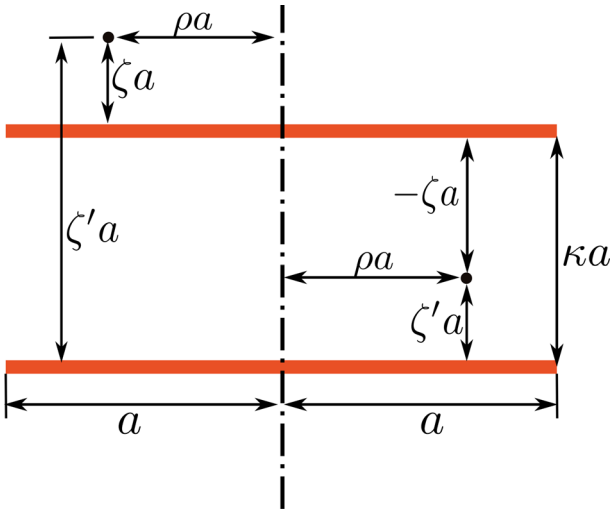

Fig. 1 A parallel plate capacitor problem with given dimensionless coordinates, ρ, ζ, ζ' and a spacing parameter, κ. Drawing is taken from [2, Fig. 1]

equation. This so-called Love's equation is solved in cylindrical coordinates in [4]. The electric potential, V, in Love's theorem is given by

$$V(\rho,\zeta)=\frac{1}{\pi}\int_{-1}^{1}\left\{\frac{1}{\sqrt{\rho^2+(\zeta+it)^2}}-\frac{1}{\sqrt{\rho^2+(\zeta'+it)^2}}\right\}f(t)\mathrm{d}x, \tag{1}$$

where both square roots have positive real part and $f(t)$ is the unique solution of the integral equation

$$f(x)-\frac{1}{\pi}\int_{-1}^{1}\frac{\kappa}{\kappa^2+(x-t)^2}f(t)\mathrm{d}t=1 \quad \text{for } -1\leqslant x\leqslant 1. \tag{2}$$

These solutions have been presented in [3]. The parameters in Eqs. (1) and (2) refer to Fig. 1.

Equation (2) is a Fredholm integral equation of the second kind and various numerical techniques have been applied to solve this integral equation [5–8]. In [9] a different analytical solution for parallel plate capacitor problem is proposed, which is criticized in [10] since it fails to satisfy all the requirements of the problem. The electric field outside the parallel plate capacitor in [11] may be captured by an explicit analytical solution as well. By reducing the system, the distance between the two plates has been simplified to vanish, such that the solution represents the electric field distribution outside the plates. A generalized Love's equation is motivated in [12] for a capacitor composed of two discs of different radii.

Capacitance is one of the basic concepts in electrodynamics measuring the performance of a capacitor by a ratio between charge and potential difference of separated plates. For example, a capacitor constructed by two parallel plates, both of area A, separated by a distance d, an "ideal" capacitance is given by

$$C=\varepsilon_0\frac{A}{d}, \tag{3}$$

where ε_0 is vacuum permittivity. Under the condition $A\gg d^2$, this simplified solution holds accurately. The case in Eq. (3) holds true whenever the area between plates is under vacuum or filled with air. When a parallel plate capacitor has a dielectric with a relative permittivity, ε_r, between the plates, then the capacitance reads

$$C=\varepsilon_0\varepsilon_\mathrm{r}\frac{A}{d}. \tag{4}$$

These ideal capacitance equations assume that the electric field is uniform and also perpendicular to the capacitor electrodes. These simple forms fail to account for fringing effect (also called edge effect). The fringing effect represents the non-uniform electric field around the edge of a parallel plate capacitor (see

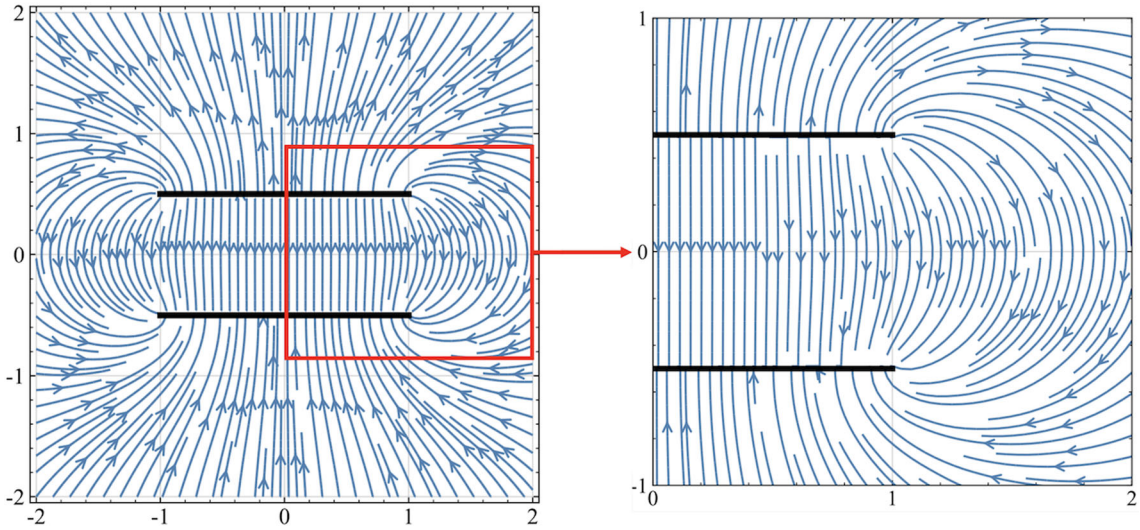

Fig. 2 Electric field distribution as obtained in Sect. 3 around the edge of a two-dimensional parallel plate capacitor model

Fig. 2). When studying a finite parallel plate capacitor problem, edge effects need to be considered in order to improve the accuracy of the capacitance results. Kirchhoff studied a circular parallel plate capacitor problem in 1877, and gave an equation for the capacitance with fringing effect [13]. Kirchhoff's equation has been proved after 85 years in [14]. Technically, the determination of the capacitance of a plate capacitor is directly related to Love's equation. In order to obtain the capacitance, different numerical and analytical approaches have been developed [15–17]. One often used technique is the small separation assumption, which is based on the simplification that two plates are separated by a very small distance regarding their lengths. A more general approach in [18] characterizes the capacitance for larger separation per length ratios. In [19] Xiang proposed a capacitance equation as shown in Eq. (5) that takes into account fringing effect for two-dimensional parallel-plate capacitor problem, which is used to verify a finite element method based numerical simulation in [20]. The λ coefficient in Eq. (5) is related to L/d. Because of the two-dimensional problem, L represents the plate length instead of the area, i.e. the length along the direction perpendicular to the two-dimensional plane, which is regarded as the unit length such that the area is $L \times 1$. In this paper we use Xiang's equation to verify our finite element results of two-dimensional parallel-plate capacitor problem and we explain the following result in detail,

$$C = -\frac{\varepsilon_0}{\pi}\Big[\ln\lambda + \ln\left(1 + 2\lambda^4 + 15\lambda^8 + 150\lambda^{34} + \cdots\right)\Big]. \tag{5}$$

The problem of a dielectric between two plates is challenging. In [21] the dynamics of the terraces on the silicon surface due to the combined effect of strain and current are investigated. In [22,23] the necessary material parameters appearing in the thermo-electric-viscoelastic constitutive model are determined experimentally and thus the relevant numerical model is developed. In some cases, for example by replacing the solid dielectric by an insulating fluid flow, the dielectric even varies between the two plates. The design of multilayer dielectrics has found application in the study of dielectric elastomer actuators [24–27]. Yet the literature lacks for studies on the problem of single/multiple dielectrics between two plates, especially in multiple dielectrics, albeit their use in electronics is quite common. For solving electric field, we use governing equations with the electric potential as a given boundary condition. As a consequence, two plates of the capacitor store equal amounts of opposite charges that create the electric potential difference and an electric field. Theoretically, the charge density may be used as a given boundary condition for such a study as well. We address the question of differences in choosing electric potential versus charge density as the boundary condition. Especially in functionalized surfaces, where the surface charge is manipulated by a coating, it is of utmost importance to comprehend the physics related to the charge and electric potential, where they are inherently coupled by Maxwell equations [28]. In reality, electrical components often work under a periodic electric field environment, which results in energy dissipation in a capacitor. At present, there are almost no literature discussing the numerical analysis of this problem.

In this work, we develop the weak form of the governing equations and solve it by the finite element method and verify the implementation by deriving an analytical solution with a single/multiple layers. The finite element model is developed by open-source packages, the FEniCS project.[1] All codes are made public on Github[2] to be used under the GNU Public license[3] for promoting an efficient scientific exchange as well as further studies. We demonstrate a verification of the numerical implementation across the length-scales, since the Maxwell equations are valid for all length-scales in continuum mechanics. By choosing boundary conditions differently, we expect building models for selectively studying various combinations of materials for dielectric and plates leading to a better understanding of the underlying mechanisms. Additionally, we calculate a capacitor's quality factor and give a transient solution that takes into account dielectric loss, which is modeled by an irreversible part of charge potential.

2 Governing equations

We begin with classical electrodynamics theory, we refer to [29–32] for a more detailed introduction. The Maxwell equations are introduced in two groups, from Faraday's law, we obtain

$$\nabla \cdot \boldsymbol{B} = 0, \ \nabla \times \boldsymbol{E} = -\frac{\partial \boldsymbol{B}}{\partial t}, \tag{6}$$

where $\boldsymbol{B}$ is the magnetic flux (area) density in T (tesla), $\boldsymbol{E}$ denotes electric field in V/mm (volt per meter). We use standard continuum mechanics notation with ∇ for grad operator meaning a space derivative and $\partial()/\partial t$ as the rate. A solution of these equations is established by the following ansatz functions:

$$\boldsymbol{E} = -\nabla\varphi - \frac{\partial \boldsymbol{A}}{\partial t}, \ \boldsymbol{B} = \nabla \times \boldsymbol{A} \tag{7}$$

with the electric potential, φ in V, and magnetic potential, $\boldsymbol{A}$ in T mm. This solution introduces gauge freedom, in other words, we may select $\nabla \cdot \boldsymbol{A}$ and $\partial\varphi/\partial t$ freely without changing the electromagnetic fields, $\boldsymbol{E}$, $\boldsymbol{B}$. From the balance of electric charge, with the charge (volume) density, q in C/mm^3 (coulomb per volume), we obtain the following Maxwell equations:

$$\nabla \cdot \boldsymbol{D} = q, \ \nabla \times \boldsymbol{H} = \boldsymbol{J} + \varepsilon_0 \frac{\partial \boldsymbol{E}}{\partial t}, \tag{8}$$

where the charge potential, $\boldsymbol{D}$ in C/mm^2, current potential, $\boldsymbol{H}$ in mA/mm (ampere per meter), and electric current (area) density, $\boldsymbol{J}$ in mA/mm^2, need to be defined by constitutive equations. The form of Maxwell equations depend on the chosen unit system and we use the Maxwell–Lorentz aether relations:

$$\boldsymbol{D} = \varepsilon_0 \boldsymbol{E}, \ \boldsymbol{H} = \frac{1}{\mu_0}\boldsymbol{B}, \tag{9}$$

where $\varepsilon_0 = 8.85 \times 10^{-12}$ mA s/(V mm) and $\mu_0 = 4\pi \times 10^{-13}$ V s/(mA mm) are universal constants. The parallel plate capacitor problem is an electrostatics problem such that magnetic potential vanishes, $\boldsymbol{A} = 0$. The total charge is composed of free and bound charges, where the free charge potential, $\mathfrak{D}$, and bound charge potential, $\boldsymbol{P}$, are introduced, as follows:

$$\boldsymbol{D} = \mathfrak{D} - \boldsymbol{P}, \tag{10}$$

where $\boldsymbol{P}$ is also known as electric polarization. For a linear material, we use

$$\mathfrak{D} = \varepsilon_0 \varepsilon_\mathrm{r} \boldsymbol{E}, \tag{11}$$

where dielectric permittivity, ε_r, is a material parameter. Therefore, from Eq. (8), we obtain

$$\nabla \cdot \mathfrak{D} = q^\mathrm{f}, \ -\frac{\partial \mathfrak{D}}{\partial t} = \boldsymbol{J}^\mathrm{f}. \tag{12}$$

[1] The FEniCS computing platform, https://fenicsproject.org/.
[2] Yiming Liu's Github account, https://github.com/liuyiming0507/FEM-for-PPC.
[3] GNU Public. Online: https://www.gnu.org/licenses/gpl-3.0.en.html.

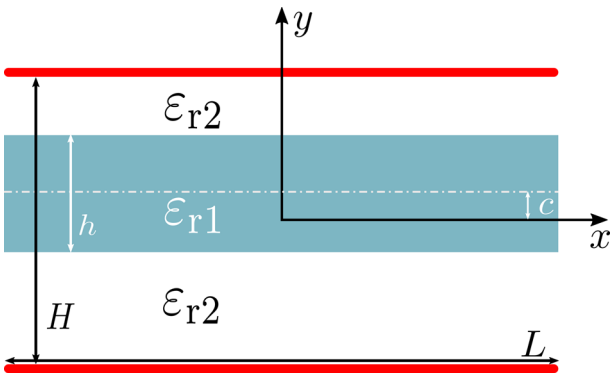

Fig. 3 An infinite parallel plate capacitor with a dielectric inside

In Eq. (12), q^{f} is the free charge per unit volume, which is different from surface charges. The electric potential is a (smooth) continuous function, but the charge potential varies for different materials (mediums) with differing permittivity, ε_{r}. The top and bottom boundaries of the dielectric are such singular interfaces, where the charge potential experiences a jump across these interfaces, see the top and bottom boundary of blue area in Fig. 3. We assume that there are no free charges on the interfaces, $q_{\mathrm{I}}^{\mathrm{f}} = 0$ and obtain

$$\begin{aligned} \boldsymbol{n} \cdot [\![\mathfrak{D}]\!] &= q_{\mathrm{I}}^{\mathrm{f}} = 0, \\ [\![\mathfrak{D}]\!] &= \mathfrak{D}^{+} - \mathfrak{D}^{-}, \end{aligned} \tag{13}$$

where $\boldsymbol{n}$ is the unit normal vector of interface and $[\![\cdot]\!]$ indicates a jump between values at either sides of the interface, $\mathfrak{D}^{\pm}$. Equivalently, by using Eq. (11), it reads

$$\begin{aligned} \boldsymbol{n} \cdot [\![\varepsilon_0 \varepsilon_{\mathrm{r}} \nabla \varphi]\!] &= 0, \\ [\![\varepsilon_0 \varepsilon_{\mathrm{r}} \nabla \varphi]\!] &= \varepsilon_0 \varepsilon_{\mathrm{r}}^{+} (\nabla \varphi)^{+} - \varepsilon_0 \varepsilon_{\mathrm{r}}^{-} (\nabla \varphi)^{-}. \end{aligned} \tag{14}$$

Within the dielectric, no free charges exist, such that motion of free charges and thus rate of free charge potential vanish. In other words, the charge potential is instantaneous and has to satisfy

$$\nabla \cdot \mathfrak{D} = 0. \tag{15}$$

Into the latter we insert Eq. (11) and obtain the well-known Laplace's equation for the electric potential,

$$\nabla^2 \varphi = 0. \tag{16}$$

3 Analytical solution

We consider an infinitely long parallel plate capacitor problem in two-dimensional continuum as illustrated in Fig. 3. The red lines are the top and bottom plates made of a conductor (metal). The origin of the coordinate system is located at the center of the capacitor. The area with the blue shadow is a dielectric material and the white dashed line is the centerline of the dielectric. The geometry is defined by the distance between the two plates, H, the thickness of the dielectric, h, and the offset of the dielectric center relative to the x-axis, c. The relative permittivities of two different media are $\varepsilon_{\mathrm{r}1}$ and $\varepsilon_{\mathrm{r}2}$. Aligned with the infinitely long capacitor along x, we assume that the problem is reduced from a two-dimensional problem to a one-dimensional problem by letting the electric potential, φ, vary only along y-direction. This simplification results in the following boundary value problem:

$$\varphi(y) = \begin{cases} \varphi_1(y), & -\dfrac{h}{2} + c < y < \dfrac{h}{2} + c, \\ \varphi_2(y), & \dfrac{h}{2} + c < y < \dfrac{H}{2}, \\ \varphi_3(y), & -\dfrac{H}{2} < y < -\dfrac{h}{2} + c. \end{cases} \tag{17}$$

The Laplace problem in Eq. (16) reads

$$\begin{gathered}\nabla^2\varphi_a = 0,\ a = 1, 2, 3,\\ \text{or,}\\ \varphi_a''(y) = 0,\ a = 1, 2, 3.\end{gathered} \tag{18}$$

By integrating twice, we obtain

$$\varphi_a(y) = \hat{C}_a y + \hat{D}_a, \tag{19}$$

with the gradient

$$\nabla\varphi_a(y) = \hat{C}_a \boldsymbol{e}_y. \tag{20}$$

$\hat{C}_a$ and $\hat{D}_a$ are coefficients. At the top interface, $y = \frac{h}{2} + c$ with $\boldsymbol{n} = \boldsymbol{e}_y$, we have as a limit value $\varepsilon_{\mathrm{r}}^{+} = \varepsilon_{\mathrm{r}2}$ and $\varepsilon_{\mathrm{r}}^{-} = \varepsilon_{\mathrm{r}1}$. With the solution in Eq. (20), we obtain $(\nabla\varphi)^{+} = \hat{C}_2$ and $(\nabla\varphi)^{-} = \hat{C}_1$. Inserting these values into Eq. (14), the transition condition at the top interface reads $\varepsilon_{\mathrm{r}2}\hat{C}_2 = \varepsilon_{\mathrm{r}1}\hat{C}_1$. Analogously, for the bottom interface, $y = -\frac{h}{2} + c$, we obtain $\varepsilon_{\mathrm{r}2}\hat{C}_3 = \varepsilon_{\mathrm{r}1}\hat{C}_1$. We summarize the transition conditions,

$$\begin{aligned}\varepsilon_{\mathrm{r}2}\hat{C}_2 &= \varepsilon_{\mathrm{r}1}\hat{C}_1,\ \forall y = \frac{h}{2} + c,\\ \varepsilon_{\mathrm{r}2}\hat{C}_3 &= \varepsilon_{\mathrm{r}1}\hat{C}_1,\ \forall y = -\frac{h}{2} + c.\end{aligned} \tag{21}$$

In order to fulfill the Laplace's equation (16) the electric potential, φ, has to be continuous in the entire domain. Therefore, on the interfaces, we obtain the continuity conditions, $\varphi_1\left(y = \frac{h}{2} + c\right) = \varphi_2\left(y = \frac{h}{2} + c\right)$ and $\varphi_1\left(y = -\frac{h}{2} + c\right) = \varphi_3\left(y = -\frac{h}{2} + c\right)$. By using them in Eq. (19), the continuity conditions read

$$\begin{aligned}\hat{C}_1\left(\frac{h}{2} + c\right) + \hat{D}_1 &= \hat{C}_2\left(\frac{h}{2} + c\right) + \hat{D}_2,\\ \hat{C}_1\left(-\frac{h}{2} + c\right) + \hat{D}_1 &= \hat{C}_3\left(-\frac{h}{2} + c\right) + \hat{D}_3.\end{aligned} \tag{22}$$

As boundary conditions, we define the electric potential as given on both plates,

$$\varphi_2\left(y = \frac{H}{2}\right) = \frac{\varphi_0}{2},\ \varphi_3\left(y = -\frac{H}{2}\right) = -\frac{\varphi_0}{2}, \tag{23}$$

leading to

$$\hat{C}_2\frac{H}{2} + \hat{D}_2 = \frac{\varphi_0}{2},\ -\hat{C}_3\frac{H}{2} + \hat{D}_3 = -\frac{\varphi_0}{2}. \tag{24}$$

By using the transition conditions in Eq. (21), continuity conditions in Eq. (22), and boundary conditions Eq. (23), we obtain for the electric potential,

$$\varphi(y) = \begin{cases}\dfrac{2\varepsilon_{\mathrm{r}2}\varphi_0}{(1-\varepsilon_{\mathrm{r}1})h + \varepsilon_{\mathrm{r}1}H}y + \dfrac{2(\varepsilon_{\mathrm{r}1} - \varepsilon_{\mathrm{r}2})}{(1-\varepsilon_{\mathrm{r}1})h + \varepsilon_{\mathrm{r}1}H}\varphi_0 c, & -\dfrac{h}{2} + c < y < \dfrac{h}{2} + c,\\ \dfrac{2\varepsilon_{\mathrm{r}1}\varphi_0}{(1-\varepsilon_{r1})h + \varepsilon_{\mathrm{r}1}H}y + \dfrac{(1-\varepsilon_{\mathrm{r}1})h}{(1-\varepsilon_{\mathrm{r}1})h + \varepsilon_{\mathrm{r}1}H}\varphi_0, & \dfrac{h}{2} + c < y < \dfrac{H}{2},\\ \dfrac{2\varepsilon_{r1}\varphi_0}{(1-\varepsilon_{\mathrm{r}1})h + \varepsilon_{\mathrm{r}1}H}y - \dfrac{(1-\varepsilon_{\mathrm{r}1})h}{(1-\varepsilon_{\mathrm{r}1})h + \varepsilon_{\mathrm{r}1}H}\varphi_0, & -\dfrac{H}{2} < y < -\dfrac{h}{2} + c.\end{cases} \tag{25}$$

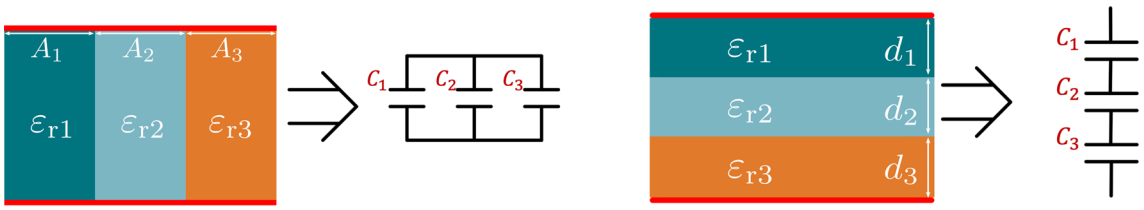

(a) Parallel connection (b) In series connection

Fig. 4 Different dielectric compositions between the plates

and thus for the electric field,

$$\boldsymbol{E}(y) = \begin{cases} -\dfrac{2\varepsilon_{r2}\varphi_0}{(1-\varepsilon_{r1})h + \varepsilon_{r1}H}\boldsymbol{e}_y, & -\dfrac{h}{2} + c < y < \dfrac{h}{2} + c, \\ -\dfrac{2\varepsilon_{r1}\varphi_0}{(1-\varepsilon_{r1})h + \varepsilon_{r1}H}\boldsymbol{e}_y, & \dfrac{h}{2} + c < y < \dfrac{H}{2} \text{ and } -\dfrac{H}{2} < y < -\dfrac{h}{2} + c. \end{cases} \tag{26}$$

We continue in order to reach the goal of getting the capacitance of this system. For the problem depicted in Fig. 3, where between plates different dielectric materials (air and dielectric material) are used, we may macroscopically divide the entire parallel plate capacitor into a parallel/series problem of several capacitors composed of a single dielectric, as shown in Fig. 4. In the case of a parallel connection in Fig. 4a, the capacitance is calculated by

$$C_a = \varepsilon_0 \varepsilon_{r\,a} \frac{A_a}{d}, \; C = \sum_{a=1}^{3} C_a. \tag{27}$$

In the case of in series connection as in Fig. 4b, the capacitance reads

$$C_a = \varepsilon_0 \varepsilon_{r\,a} \frac{A}{d_a}, \; \frac{1}{C} = \sum_{a=1}^{3} \frac{1}{C_a}. \tag{28}$$

We propose to use these simplified calculations above, since the Laplace problem is a linear differential equation and the superposition principle holds. These results are used to verify the numerical solutions in the following.

4 Computational implementation

The finite element method (FEM) is used by following implementations in [33,34] and refer to [35, Sect. 3] for engineering examples in electromagnetism by using FEniCS packages. Herein, we implement two FE models: the finite parallel plate capacitor in Fig. 5a and the infinite parallel plate capacitor in Fig. 5b; both of them as two-dimensional problems with upper and lower plates treated as interfaces. The computational domain, Ω, is composed of Ω_1 and Ω_2 representing two different mediums, $\Omega = \Omega_1 \cup \Omega_2$. The closure of the domain, $\partial\Omega$, is the boundary to be defined by additional conditions. For the finite plate problem, a sufficiently large domain is needed to ensure that the FEM corresponds to the analytical solution. In the case of the infinite plate problem, periodic boundary conditions are used on left and right sides reducing the size of the computational domain significantly. In other words, the solution space is constructed with a restriction that the solution on left and right ends are identical. Thus, the mesh needs to be utilized in such a way that the vertical coordinates of nodes on the left are matching the vertical coordinates on the right. Periodic boundary conditions are used to model infinity only along the x-direction in Fig. 5b.

Boundaries are denoted by $\Gamma_1, \Gamma_2 \ldots \Gamma_7$. By using a variational formulation, we begin with the governing equation (15), multiply by an arbitrary test function, $\delta\varphi$, and obtain an integral form within the domain composed of finite sized domains Ω^{E} called elements,

$$\sum_{\mathrm{E}} \int_{\Omega^{\mathrm{E}}} \nabla \cdot \mathfrak{D} \delta\varphi \, \mathrm{d}v = 0. \tag{29}$$

The electric potential, φ, is the unknown variable and the constitutive equation (30) involves first gradient of φ already,

$$\mathfrak{D} = -\varepsilon_0 \varepsilon_\mathrm{r} \nabla \varphi. \tag{30}$$

The integral form incorporates second-order partial derivatives of φ, whereas no derivatives of $\delta\varphi$. According to the Galerkin procedure, we may use the same space for φ and $\delta\varphi$ such that we choose to weaken the continuity condition by integrating by parts and applying Gauß's theorem,

$$\sum_\mathrm{E} \int_{\partial\Omega^\mathrm{E}\setminus I} \delta\varphi \mathfrak{D} \cdot \boldsymbol{n}\, \mathrm{d}s + \int_I \delta\varphi \boldsymbol{n} \cdot [\![\mathfrak{D}]\!] \mathrm{d}S - \sum_\mathrm{E} \int_{\Omega^\mathrm{E}} \mathfrak{D} \cdot \nabla\delta\varphi \mathrm{d}v = 0. \tag{31}$$

We emphasize the used notation;

- Between elements, I represents the interface used herein modeling the upper and lower plates. The sum over elements introduces the jump brackets since neighboring elements have oppositely directed surface normals, $\boldsymbol{n}$, on the shared surface.
- The sum over elements let the terms on shared boundaries vanish since $\mathfrak{D}$ is continuous except on the interface.
- With a sum over elements $\sum_\mathrm{E} \partial\Omega^\mathrm{E}\setminus I = \partial\Omega$ represents Lipschitz boundaries, which is sufficiently regular and possesses only outer boundaries.
- Within the domain, we obtain after assemble, $\sum_\mathrm{E} \Omega^\mathrm{E} = \Omega$.

In the Sect. 2, we assumed that the charge on the interface is 0, where the interface referred to the interface between different media. But in this section, I refers specifically to two plates, where we have no zero charge assumption. Therefore, how the second term in the Eq. (31) is handled depends on different boundary conditions, which is explained in detail below.

The standard FEM elements are employed [36], they are of order q and span $\mathcal{P}_q$ on Ω^E. Shape functions are piecewise or elementwise continuous over the whole domain with a compact support on the element such that nodal values have influence only locally. This representation is adequate for approximation in Hilbertian Sobolev space $\mathcal{H}^1$. Piecewise continuity ensures a monotonic convergence. Linear Lagrange elements are used for φ, which means we use interpolation polynomial of first order as shape function for each element in scalar space,

$$\mathcal{V} = \left\{ \varphi \in \mathcal{H}^1(\Omega) : \varphi\Big|_{\Omega^\mathrm{E}} \in \mathcal{P}_1(\Omega^\mathrm{E})\ \forall \Omega^\mathrm{E} \in \mathcal{T} \right\}. \tag{32}$$

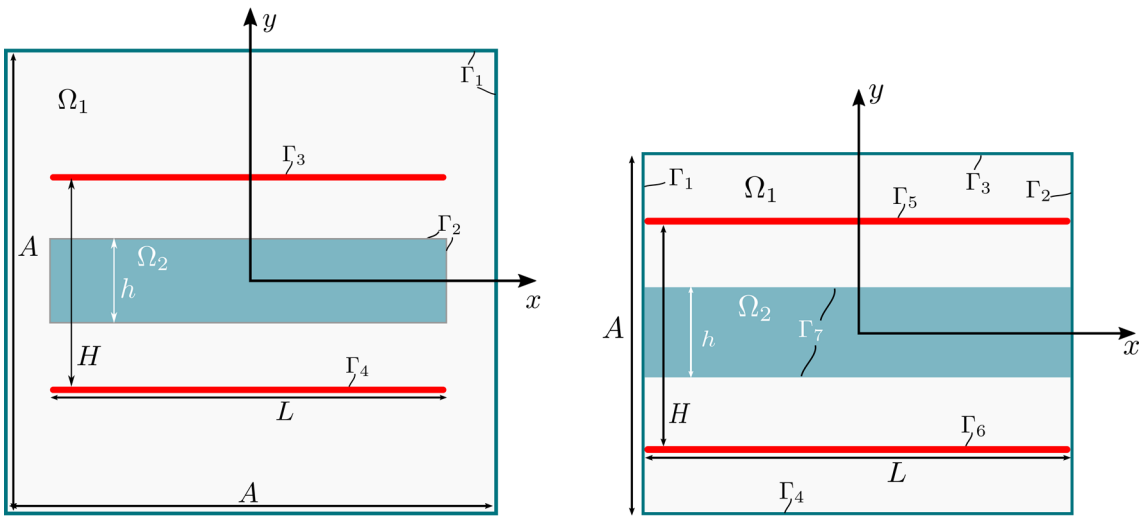

(a) Finite parallel plate capacitor. (b) Infinite parallel plate capacitor.

Fig. 5 The two studied FE models, (**a**) and (**b**) are tow models, both of them used in Case A and Case B. The geometry is symmetric along the x and y axes

In addition, because of the existence of dielectric, $\mathfrak{D}$ is piecewise continuous in vector space. We choose discontinuous Lagrange elements for $\mathfrak{D}$, which implies L^2 elements with $\mathcal{P}_0$ such that they generate a constant within the element with a jump across the boundaries. We emphasize of not using any special elements [37] designed for electromagnetism herein. Therefore, an extension in multiphysics as in [38,39] is straightforward that is a benefit of the presented formulation.

In Eq. (31), the integral over the interface, I, is related to the charge density on the interface. For implementation of this term, we introduce two distinct cases:

A: We use the electric potential, φ, as given on the two plates (interface). This so-called Dirichlet boundary condition let the boundary term vanish. since $\delta\varphi = 0$ is set on Dirichlet boundaries.
B: Instead, we may apply a charge density as a Neumann boundary condition and observe the significance of this term.

Next, we will clarify these two boundary conditions (case A and case B) separately.

4.1 Case A: Electric potential boundary condition

As we use Dirichlet boundary condition on the interface, its solution is given such that the nodes are taken out of the system, in other words, the numerical implementation circumvents from solving the values on the corresponding degrees of freedom. The weak form (31) simplifies to

$$\int_{\partial\Omega} \delta\varphi \mathfrak{D} \cdot \boldsymbol{n} \mathrm{d}s - \int_{\Omega} \mathfrak{D} \cdot \nabla\delta\varphi \mathrm{d}v = 0. \tag{33}$$

For the model as depicted in Fig. 5a, on Γ_1 we set $\varphi\big|_{\Gamma_1} = 0$ to simulate zero potential at infinity—this boundary, Γ_1, denotes the boundary of the whole computational domain. Hence, we need a sufficiently large domain in order to incorporate this far-away boundary condition correctly. Γ_2 is the boundary between two different media, Ω_1 and Ω_2, i.e. the boundary of a dielectric in vacuum or the boundary between different dielectrics. Because of insulators, there is no free charge on this boundary, in other words, the jump condition vanishes. Interface is composed of Γ_3 and Γ_4 representing the upper and lower plates, respectively. On the upper plate Γ_3, we have $\varphi\big|_{\Gamma_3} = \frac{\varphi_0}{2}$ and on the lower plate Γ_4 we have $\varphi\big|_{\Gamma_4} = -\frac{\varphi_0}{2}$.

For the model as seen in Fig. 5b, in order to involve an infinitely long plate configuration, we use a periodic boundary condition $\varphi\big|_{\Gamma_1} = \varphi\big|_{\Gamma_2}$ on the left and right boundaries, Γ_1 and Γ_2, respectively. $\varphi\big|_{\Gamma_1} = \varphi\big|_{\Gamma_2}$ means mapping the values on the left boundary to the right boundary. In other words, each degree of freedom on the left corresponds to one degree of freedom on the right, their vertical coordinates are equal such that their values to be solved are set to be equal as well. This restriction is directly implemented in the functional space. Γ_3, Γ_4 are the top and bottom boundaries of the domain, with the analogous far-away condition of $\varphi\big|_{\Gamma_3\cup\Gamma_4} = 0$ [40]. And on two plates Γ_5, Γ_6 we have $\varphi\big|_{\Gamma_5} = \frac{\varphi_0}{2}$ and $\varphi\big|_{\Gamma_6} = -\frac{\varphi_0}{2}$. Γ_7 is a set of boundaries between different insulating media, where the jump of charge potential vanishes.

4.2 Case B: Charge density boundary condition

The charge stored on the plate is the source of the electric potential. In order to introduce the charge density on the two plates as the boundary condition, we need to change the second part in Eq. (31) and introduce the following relationship:

$$q^{\mathrm{f}} = \boldsymbol{n} \cdot [\![\mathfrak{D}]\!] = \boldsymbol{n} \cdot \left(\mathfrak{D}^{+} - \mathfrak{D}^{-}\right), \tag{34}$$

where q^{f} is the charge density. We fail to obtain q^{f} directly from Eq. (34) in FEM, but we may easily calculate the integral over the interface in order to obtain the total charge:

$$Q = \int_I q^{\mathrm{f}} \, \mathrm{d}S. \tag{35}$$

Q is the total charge on one plate and another plate carries the same amount of negative charge. For having cases A and B identical, the total charge, Q, is calculated from the results acquired by solving Eq. (33) in Case A.

Substituting Eq. (34) into the second part of Eq. (31), we get the weak form for Case B,

$$\int_{\partial\Omega} \delta\varphi \mathfrak{D} \cdot \boldsymbol{n} \mathrm{d}s + \int_I \delta\varphi \, q^{\mathrm{f}} \mathrm{d}S - \int_\Omega \mathfrak{D} \cdot \nabla\delta\varphi \mathrm{d}v = 0. \tag{36}$$

For the charge density boundary condition, we simulate Fig. 5b. Because charge distribution on an infinite parallel plate capacitor is uniform, the charge density is simply found by $q^{\mathrm{f}} = Q/L$, where $L = \int_I \mathrm{d}S$ is the length of Γ_5 and Γ_6. The charge density boundary conditions read

$$\begin{aligned} q^{\mathrm{f}} &= Q/L \quad \forall (x, y) \in \Gamma_5, \\ q^{\mathrm{f}} &= -Q/L \; \forall (x, y) \in \Gamma_6. \end{aligned} \tag{37}$$

5 Results

Capacitance is an important physical quantity for parallel plate capacitors and it is also one of the results in focus. We already have elementary relations on Eq. (27) and Eq. (28) to get reference values of capacitance. In FEM we need to calculate capacitance from the electric field results that we have solved. First, we introduce the electric field energy. It is the energy contained in an electric field. The energy density or energy per unit volume of an electric field becomes

$$u_{\mathrm{E}} = \frac{1}{2} \mathfrak{D} \cdot \boldsymbol{E} = \frac{\varepsilon_0 \varepsilon_{\mathrm{r}}}{2} |\boldsymbol{E}|^2. \tag{38}$$

The total energy U_{E} stored in electric field with the domain, Ω, is

$$U_{\mathrm{E}} = \frac{1}{2} \int_\Omega \varepsilon_0 \varepsilon_{\mathrm{r}} |\boldsymbol{E}|^2 \mathrm{d}v. \tag{39}$$

In addition, the total electric energy stored in a capacitor is given by

$$U_{\mathrm{E}} = \frac{1}{2} C V^2, \tag{40}$$

where C is the capacitance and V is the electric potential difference between the two plates. Using Eqs. (39) and (40) we get the final equation:

$$C = \frac{1}{V^2} \int_\Omega \varepsilon_0 \varepsilon_{\mathrm{r}} |\boldsymbol{E}|^2 \mathrm{d}v. \tag{41}$$

With the electric field distribution results solved by the FEM, we easily calculate Eq. (41) for obtaining the capacitance, C. Taking model (a) as an example, we select the volume between the two plates as the calculation area. As shown in the Fig. 6, Eq. (41) becomes

$$C = \frac{1}{V^2} \int_{\Omega_1' \cup \Omega_1'' \cup \Omega_2} \varepsilon_0 \varepsilon_{\mathrm{r}} |\boldsymbol{E}|^2 \mathrm{d}v. \tag{42}$$

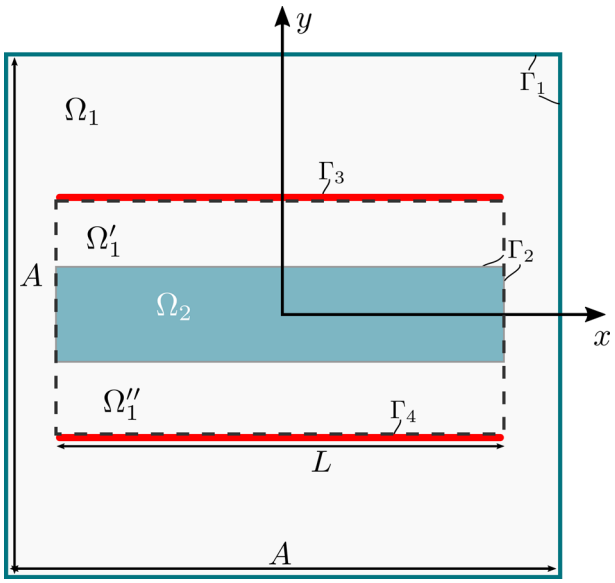

Fig. 6 Schematic diagram of the integral area indicated by the dashed line for calculating the capacitance

Table 1 Parameters setting for the analytical solution, L—length of the plates. In the FE model (b) (Fig. 5b) the domain size along y-direction $A = 50$

Parameters	Values
H(mm)	3
h(mm)	1
c(mm)	0.5
L(mm)	5
ε_{r}	$\varepsilon_{\mathrm{r1}} = 1,\ \varepsilon_{\mathrm{r2}} = 5$

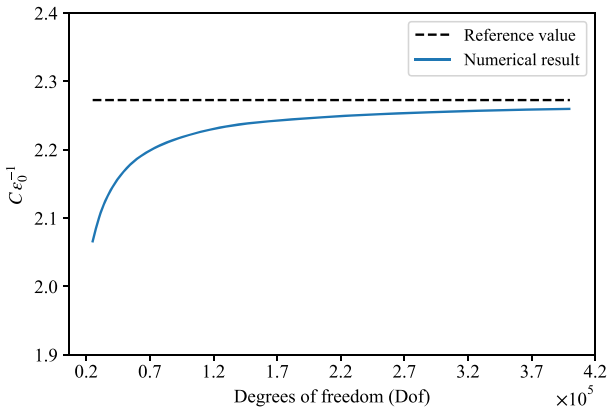

Fig. 7 Comparison of capacitance results. The reference value is from Eq. (28) and the numerical result is from Eq. (41)

5.1 Comparison between analytical and numerical solutions

Infinite parallel plate capacitor model in Fig. 5b has been studied with the parameters as compiled in Table 1 referring to Fig. 3.

We compare the capacitance computed by the numerical solution using different mesh sizes to the analytical solution. We use degrees of freedom (Dofs) in order to represent the size of mesh. As known as the h-convergence study, we increase degrees of freedom by preserving the element quality and the result in Fig. 7 indicates that the numerical solution is monotonously converging to the reference solution that is herein the analytical solution from Eq. (28). The difference is caused by Eq. (28) since we use different dielectrics and

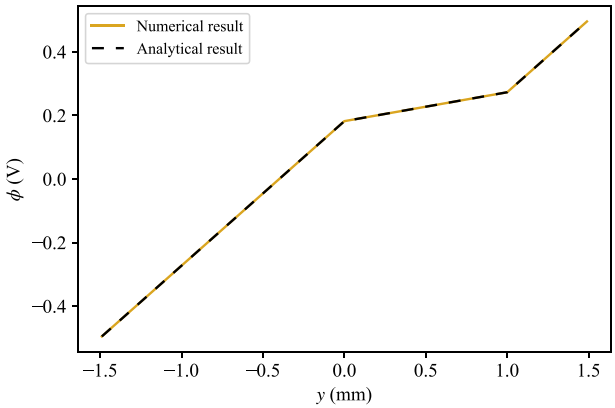

(a) The electric potential at $x = 0$.

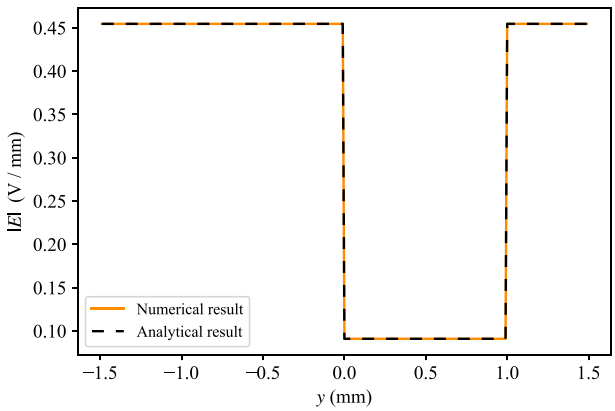

(b) The electric magnitude at $x = 0$.

Fig. 8 Comparison of φ and E at $x = 0$ along y-axis. Analytical results from Eqs. (25) and (26). Numerical results by solving Eq. (33)

series connections for the estimation. The comparison over one value may be misleading, therefore, we analyze the solution in the whole domain. We compare the electric potential and electric field results between two plates at $x = 0$ along y-axis. In Fig. 8 we observe that the numerical solution results match the analytical solution in the whole domain.

For the finite parallel plate capacitor problem, model (a), we compare the results herein with a numerical result that is presented in [6] of Love's potential equation (1). We study two different capacitors regardless of the dielectric with $L/h = 2$ and $L/h = 20$ (L—length of the plates, H—distance between the two plates) according to [6]. The comparison of the equipotential lines results is shown in Fig. 9. As shown in Fig. 9, we specify the same level of equipotential lines as in [6]. The distributions of equipotential lines obtained by the two different methods are almost identical.

For the capacitance, we compare FEM result with Xiang's equation:

$$C = -\frac{\varepsilon_0}{\pi}\left[\ln\lambda + \ln\left(1 + 2\lambda^4 + 15\lambda^8 + 150\lambda^{34} + \cdots\right)\right] \tag{43}$$

and

$$\lambda = \frac{1 - \sqrt{\tanh\frac{\pi L}{2h}}}{2\left(1 + \sqrt{\tanh\frac{\pi L}{2h}}\right)}, \tag{44}$$

where L is the length of the plate, h is the distance between the two plates. Equation (44) implies that $\lambda < 1/2$ because $0 < \tanh(\pi L/2h) < 1$. The power series on the right side of Eq. (43) converges very quickly and we

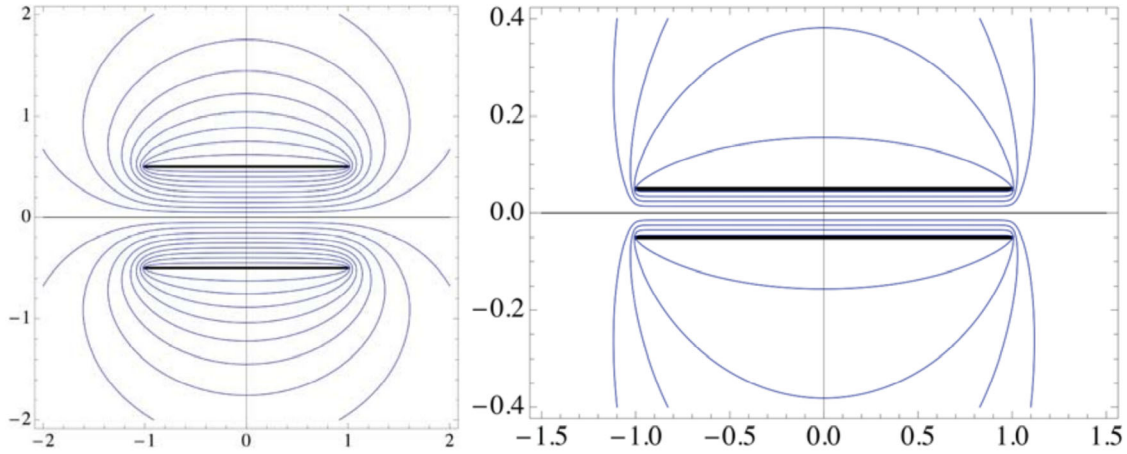

(a) Equipotential lines results in [6], $L/h = 2$ (left) and $L/h = 20$ (right).

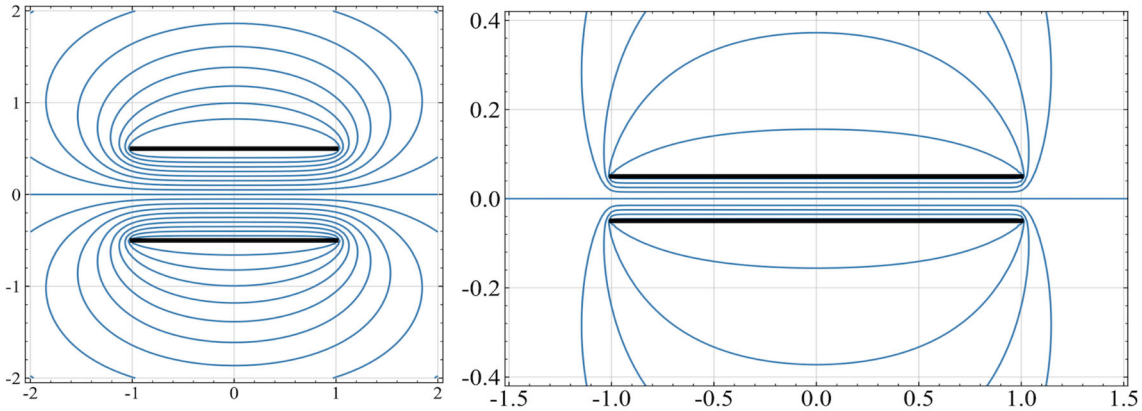

(b) FEM equipotential lines results in this paper, $L/h = 2$ (left) and $L/h = 20$ (right).

Fig. 9 Comparison of FEM solution (**b**) and a numerical solution of Love's potential equation (**a**) presented in [6]. Equipotential lines for $|V| = 0.1(0.1)0.9$ when $L/h = 2$ (left, both (**a**) and (**b**)) and for $|V| = 0.3(0.2)0.9$ when $L/h = 20$ (right, both (**a**) and (**b**))

have chosen to include four terms, as follows:

$$C = -\frac{\varepsilon_0}{\pi}\left[\ln\lambda + \ln\left(1 + 2\lambda^4 + 15\lambda^8 + 150\lambda^{34}\right)\right]. \tag{45}$$

The comparison of our FEM capacitance results and capacitance from Eq. (45) is shown in Fig. 10. On the x-axis, we use L/h representing the ratio of the plate length to the distance between the two plates. The larger L/h means that the parallel plate capacitor becomes flatter and we observe that the two results agree better.

We conclude to have verified the accuracy of the finite element model proposed in this paper. Both the potential and capacitance results show good agreement with the analytical solutions for both infinite and finite parallel plate capacitor problems. It should be pointed out that for the finite plate problem neither Love's equation nor Xiang's equation considers the presence of a single layer or multiple layers between two plates. In other words, the above equation only applies when the material between the two plates is homogeneous and its relative permittivity is $\varepsilon_r = 1$. We may calculate the capacitance of a capacitor with a single layer or multiple layers according to Eqs. (27) and (28). As mentioned before, these two simple equations do not account for edge effects, so the results are less accurate for the finite parallel plate capacitor problem. For this kind of problem, FEM shows good adaptability and flexibility, since the proposed implementation not only allow to study the presence of various dielectric layers between parallel plate capacitors, but also have the potential to study the dielectric layers with irregular shapes. Next we study the capacitance of parallel plate capacitors with multilayer dielectrics and use the analytical results of Eqs. (27) and (28) as reference.

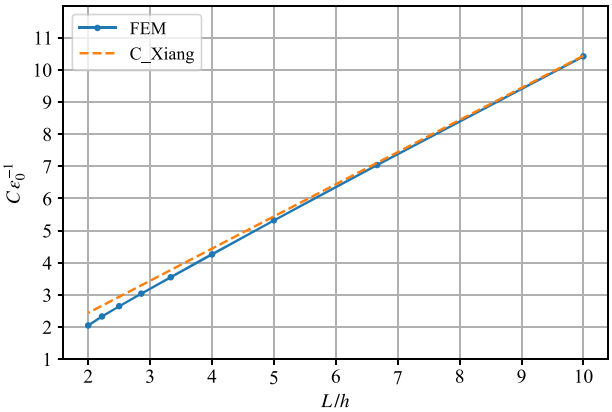

Fig. 10 FEM capacitance results vs Xiang's capacitance results from Eq. (45)

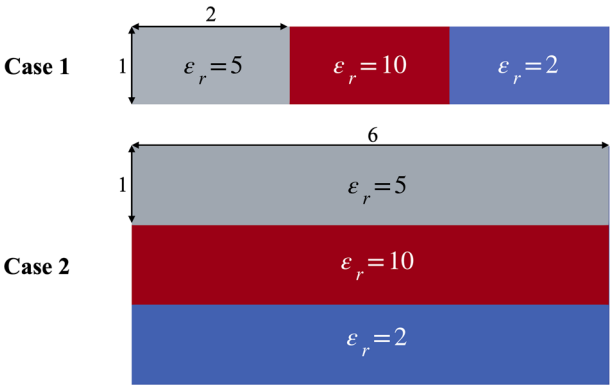

Fig. 11 Dielectrics distribution of two cases. The area between the two plates are for reference, Ω_1', Ω_1'', Ω_2 in Fig. 6. The size of the parallel plate capacitor ($L \times H$) in Case 1: 6×1 (mm^2), in Case 2: 6×3 (mm^2)

Table 2 Capacitance results in comparison between numerical results and analytical results of Case 1 and Case 2

		Capacitance (F)—Case 1	Capacitance (F)—Case 2
Numerical results	Dofs = 160 801	$34.016\varepsilon_0$	$7.538\varepsilon_0$
	Dofs = 361 201	$34.018\varepsilon_0$	$7.538\varepsilon_0$
	Dofs = 641 601	$34.019\varepsilon_0$	$7.539\varepsilon_0$
Analytical results		$34\varepsilon_0$	$7.5\varepsilon_0$

For multilayer dielectrics, we study two cases, where the difference between them is the diverse distribution of dielectrics in the capacitor as shown in the Fig. 11. For these cases we set the size of domain $A = 20\,\text{m}$ referring to Fig. 5a. This size is large enough compared to the size of the parallel plate capacitor in the two cases. And the capacitance results are shown in Table 2. Numerical and analytical results are quantitatively the same. When compared with the analytical results, the numerical capacitance results obtained by FEM used in this paper are larger in Table 2. We understand that the FEM considers fringing effects correctly where it is expected to obtain larger results because of the electric field concentration around the edges. The difference between the FEM and ideal capacitance results of Case 2 is slightly larger than that of Case 1, because the H/L of Case 2 ($H/L = 0.5$) is larger than Case 1 ($H/L = 1/6$), and the fringing effects increase as H/L increases. We visualize the electric field for presenting the fringing effects in Fig. 12, where electric field magnitude distribution indicates the concentration at the ends of the plates.

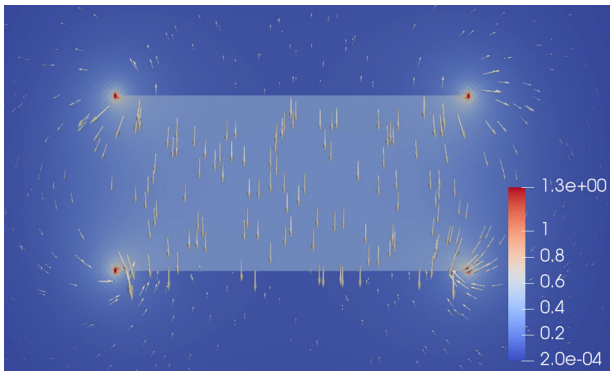

Fig. 12 Case 2 results, electric field, $\boldsymbol{E}$ in V/mm, distribution indicated by colors denoting the magnitude and scaled arrows representing the direction

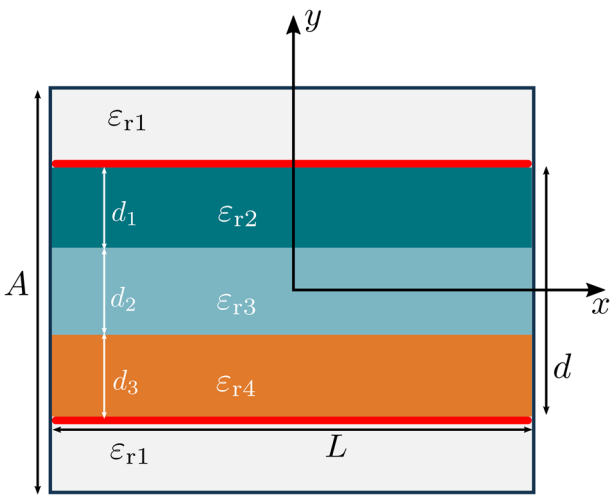

Fig. 13 More detailed geometric model based on model (b) (Fig. 5b)

Table 3 Geometric parameters and permittivities used in Case 1 and 2, see Fig. 13 for parameters' meaning

Parameters	Case 1	Case 2
L (mm)	5	5
A (mm)	50	50
d (mm)	$d = 3,\ d_1 = d_2 = d_3 = 1$	$d = 3,\ d_1 = d_2 = d_3 = 1$
ε_r	$\varepsilon_{r1} = 1,\ \varepsilon_{r3} = 4,\ \varepsilon_{r2} = \varepsilon_{r4} = 2$	$\varepsilon_{r1} = 1,\ \varepsilon_{r3} = \varepsilon_{r2} = \varepsilon_{r4} = 5$

5.2 Comparison of two different boundary conditions' implementations in the multilayer approach

We use a similar configuration as before, but this time a multilayer setting as the geometry is shown in Fig. 13. We choose a $A \gg d$ such that the simulation corresponds to an infinitely large plate along the y-direction. Parameters are compiled in Table 3.

Initially, we solve Eq. (33) under electric potential boundary conditions in order to obtain the electric potential and electric field results. Then, we calculate the total charge, Q, on one plate by means of Eqs. (34), (35). We use this total charge result as the value of Q in Eq. (37). In spite of, we use different boundary conditions, they are theoretically equivalent and the two results should be the same under ideal conditions.

The results are shown in Table 4 and Fig. 14. We observe that the difference between the results of two boundary conditions is around 1% of relative error. We stress that the charge density BD includes a numerical rounding error because of calculating Q and 1% error is reasonable to claim that the error is caused solely by this fact.

Table 4 Capacitance results in comparison between electric potential boundary condition and charge density boundary condition

Type	Capacitance (F)—Case 1	Capacitance (F)—Case 2
Electric potential BD	$3.999\varepsilon_0$	$6.667\varepsilon_0$
Charge density BD	$3.933\varepsilon_0$	$6.599\varepsilon_0$
Reference	$4.000\varepsilon_0$	$6.66\bar{6}\varepsilon_0$

5.3 A transient solution by including dielectric loss

The computational implementation is generic to be used in three-dimensional continuum as well as ready for parallelization by using *mpirun*. Therefore, industrial applications may be simulated as well. We construct the C2220 capacitor in Fig. 15, where the material of two plates are made of copper and the relative permittivity of copper is $\varepsilon_{\mathrm{r}}^{\mathrm{Cu}} = 1$ since it is an electric conductor. We choose PTFE (commercial name is Teflon given by DuPont de Nemours, Inc.) as dielectric with relative permittivity $\varepsilon_{\mathrm{r}}^{\mathrm{PTFE}} = 2.1$. We simulate a transient response by a harmonic boundary condition, where the maximum amplitude distribution may be depicted in Fig. 16.

For time varying electric fields, flux of the electric energy is reversed leading to a necessity of dielectrics also as mechanically supports in separating electrical conductors. The mechanical deformation of dielectrics creates losses in this energy transfer modeled as propagating waves. A possible model relies on permittivity,

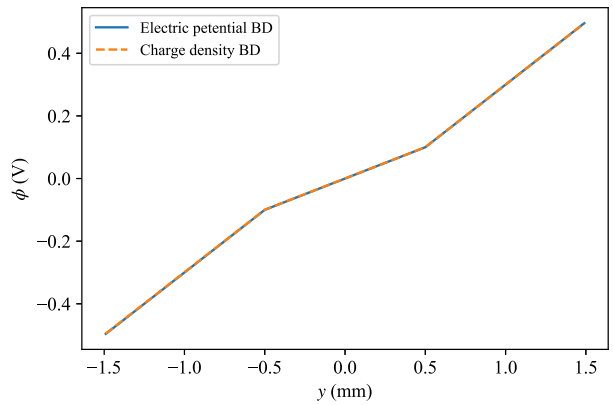

(a) The electric potential.

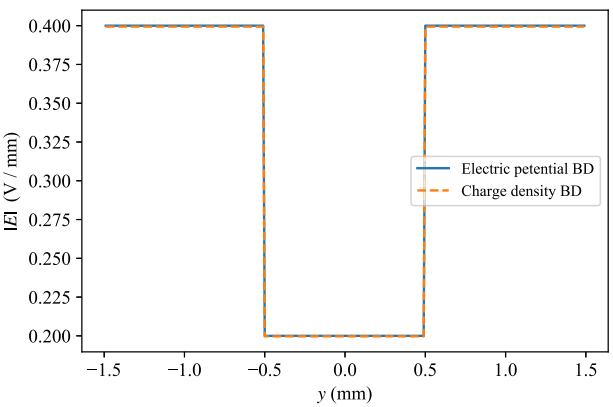

(b) The electric magnitude.

Fig. 14 Comparison of φ and E at $x = 0$ along y-axis in Case 1. The electric potential boundary condition results from Eq. (33). The charge density boundary condition results from Eq. (36)

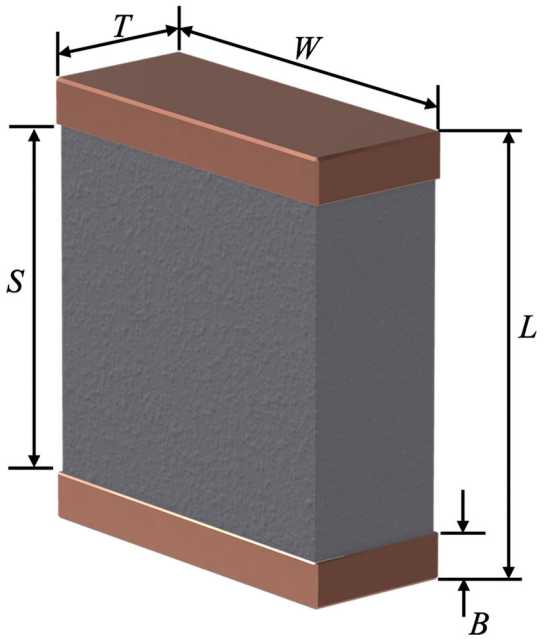

Fig. 15 Geometric parameters of C2220: $L = 5.7$ (mm), $W = 5.0$ (mm), $T = 2$ (mm), $B = 0.6$ (mm), $S = 4.5$ (mm)

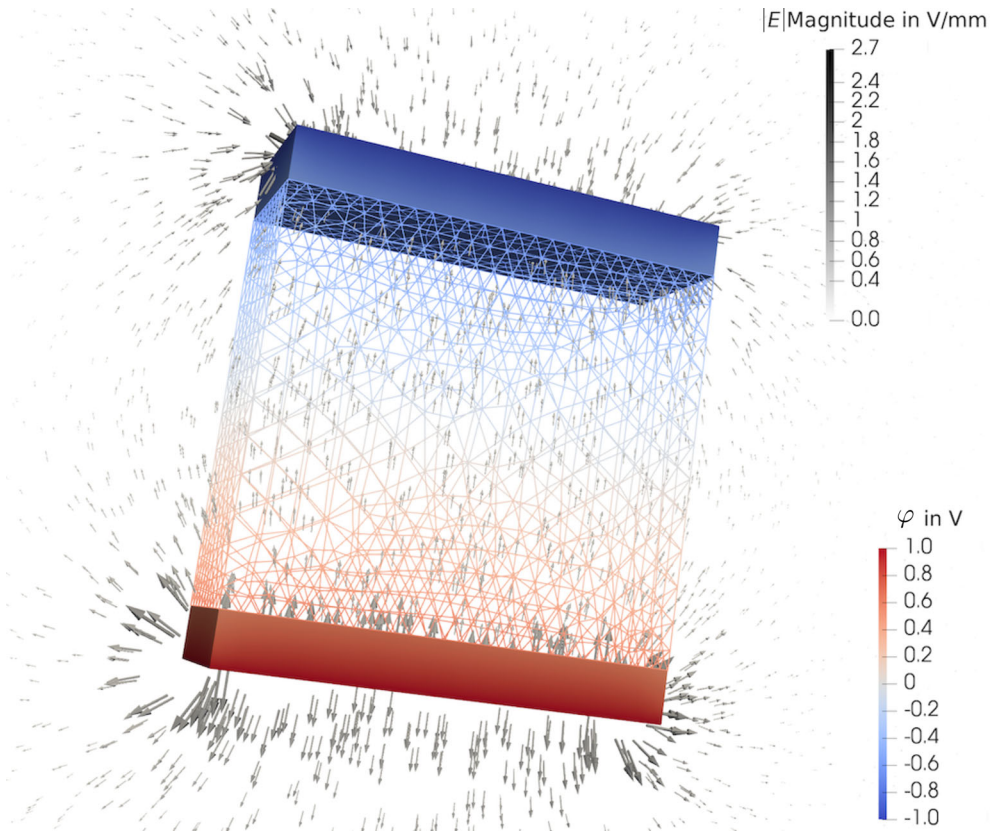

Fig. 16 A 3D example: PTFE dielectric is visualized as wireframe and the copper plates as surfaces. The capacitor is colored by φ (V). The electric field is visualized by arrows that are scaled by the $\boldsymbol{E}$ magnitude, $\|\boldsymbol{E}\|$ (V/mm), on cut planes

ε, with as a complex value with real and imaginary components,

$$\varepsilon = \varepsilon' + i\varepsilon'' = \varepsilon_0\varepsilon_\mathrm{r}' + i\varepsilon_0\varepsilon_\mathrm{r}''. \tag{46}$$

The purpose is to model the electric field as a harmonic function by using the Euler equation,

$$\boldsymbol{E} = \boldsymbol{E}_\mathrm{amp}\exp(i\omega t), \tag{47}$$

where E_amp is electric field amplitude. Equation (11) is rewritten as

$$\mathfrak{D} = \varepsilon_0\varepsilon_\mathrm{r}'\boldsymbol{E} + i\varepsilon_0\varepsilon_\mathrm{r}''\boldsymbol{E}, \tag{48}$$

by employing the rate, $\boldsymbol{E}^\cdot = i\omega\boldsymbol{E}_\mathrm{amp}\exp(i\omega t) = i\omega\boldsymbol{E}$, into Eq. (48),

$$\mathfrak{D} = \varepsilon_0\varepsilon_\mathrm{r}'\boldsymbol{E} + \varepsilon_0\frac{\varepsilon_\mathrm{r}''}{\omega}\boldsymbol{E}^\cdot. \tag{49}$$

This material model is clearly considering the reversible part as before as well as a rate term that incorporates losses in a cyclic electric loading. We may rewrite by separating reversible and irreversible (dissipative) terms

$$\begin{aligned} \mathfrak{D} &= \mathfrak{D}_\mathrm{rev} + \mathfrak{D}_\mathrm{diss}\ , \\ \mathfrak{D}_\mathrm{rev} &= \varepsilon_0 e_1\boldsymbol{E}\ ,\ \mathfrak{D}_\mathrm{diss} = \varepsilon_0 e_2\boldsymbol{E}^\bullet\ , \end{aligned} \tag{50}$$

where $e_1 = \varepsilon_\mathrm{r}'$ and $e_2 = \varepsilon_\mathrm{r}''/\omega$. For the computational implementation, we apply the finite difference method, also known as Euler-backward approach,

$$\mathfrak{D}_\mathrm{diss} = \varepsilon_0 e_2\frac{\boldsymbol{E} - \boldsymbol{E}^0}{\Delta t}, \tag{51}$$

where time step, Δt, is set constant for the sake of simplicity. One time step before, the electric potential is calculated, φ^0, which is then used for obtaining $\boldsymbol{E}^0$. By using Eq. (51) for $\mathfrak{D}$ in Eq. (33), we achieve a simulation with choosing the time-varying electric potential boundary condition $\varphi\big|_{\Gamma_5} = \frac{\varphi_0}{2}\sin(2\pi t)$ and $\varphi\big|_{\Gamma_6} = -\frac{\varphi_0}{2}\sin(2\pi t)$ by referring to Fig. 5b and solving for different values of e_2 in one circle, we plot the hysteresis curve in Fig. 17. Indeed, these dielectric losses are unwanted in design. Therefore, a quality factor is used in a capacitor, also known as the Q-factor, representing the efficiency of a given capacitor in terms of energy losses

$$Q_\mathrm{c} = \frac{W_\mathrm{rev}}{W_\mathrm{diss}}. \tag{52}$$

Herein we denote the quality factor by Q_c to distinguish it from the total charge notation. Quality factor Q_c of a parallel plate capacitor is then studied using Teflon as the dielectric. In the microwave region at a working frequency of $\omega = 10\,\mathrm{GHz}$, Teflon has an approximate real part of the relative permittivity $\varepsilon_\mathrm{r}' \approx 2.03$ and a approximate imaginary part $\varepsilon_\mathrm{r}'' \approx 0.0008$ according to [41]. We choose the time-varying electric potential boundary condition $\varphi\big|_{\Gamma_5} = \frac{\varphi_0}{2}\sin(\omega t)$ and $\varphi\big|_{\Gamma_6} = -\frac{\varphi_0}{2}\sin(\omega t)$. We define Q_c by Eq. (52), by calculating the reversible energy in one cycle

$$W_\mathrm{rev} = \int_0^{2\pi/\omega}\int_\Omega \mathfrak{D}_\mathrm{rev}\cdot\boldsymbol{E}^\cdot \mathrm{d}v\mathrm{d}t, \tag{53}$$

as well as the dissipated energy in this cycle

$$W_\mathrm{diss} = \int_0^{2\pi/\omega}\int_\Omega \mathfrak{D}_\mathrm{diss}\cdot\boldsymbol{E}^\cdot \mathrm{d}v\mathrm{d}t. \tag{54}$$

We obtain the quality factor of this parallel plate capacitor, C2220 with Teflon as the dielectric at a working frequency of 10 GHz as $Q_\mathrm{c} = 1652$. Obviously, dissipation in each cycle means an energy loss and a capacitor storing an energy has a better quality if the dissipation goes to zero meaning $Q_\mathrm{c} \to \infty$. In industrial applications, datasheet for a component has an indication about this value for a target frequency, for example good quality capacitors reach at 1 MHz over $Q_\mathrm{c} > 10\,000$ or for 1 GHz over $Q_\mathrm{c} > 1\,000$. By using a transient analysis, we demonstrate that it is straightforward to calculate this value for different frequencies. We stress that the frequency changes Q_c value.

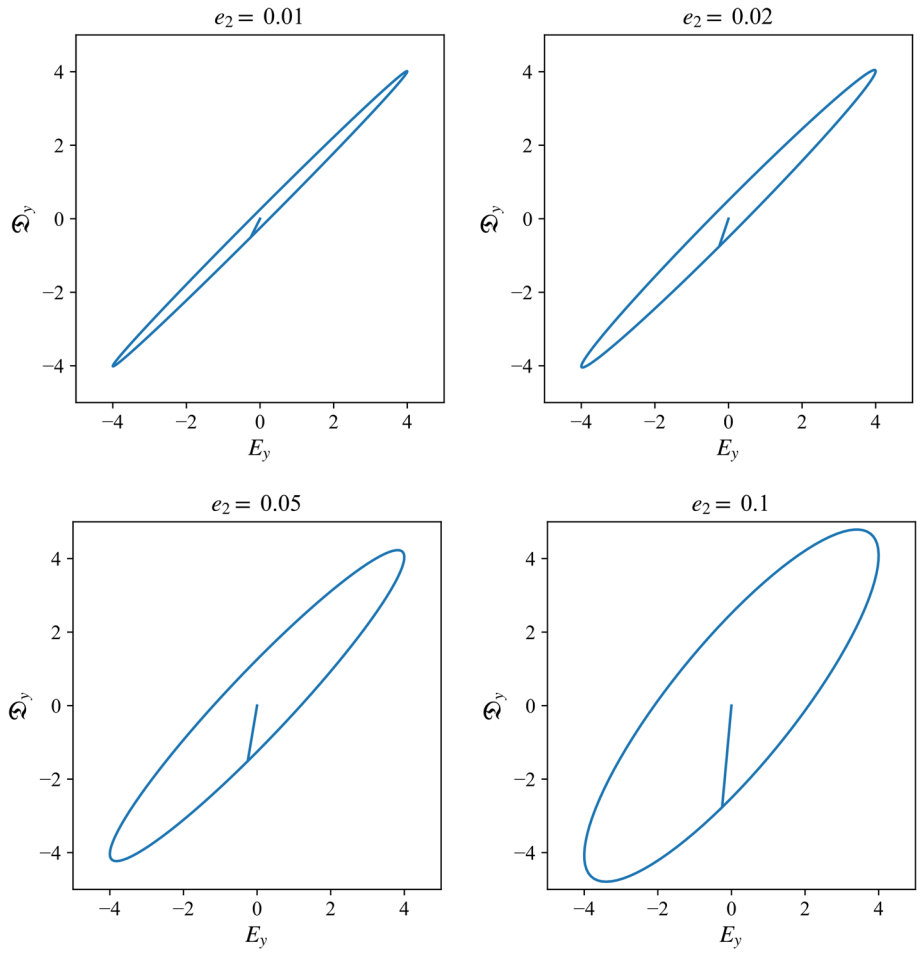

Fig. 17 Hysteresis curve for different e_2, by increasing the value of e_2 the loss energy (area of the ellipse) increases. On the x-axis, we use $\boldsymbol{E}_y$ evaluated in the middle of the computational domain, and on the y-axis, we use $\mathfrak{D}_y$ evaluated at the same position over time

6 Conclusions and outlook

In this paper we have scrutinized the weak form of an electrostatic problem in the case of surface charges. Surface charge modeling is of importance on interfaces between phases or different materials exchanging electric charges, but a numerical implementation is difficult to find in the literature [42,43]. The governing equations for electrostatic problems are solved by the finite element method (FEM) in order to study the parallel plate capacitor problem. With a choice of a "simple" problem, we have been using an analytical solution to quantify the accuracy of the numerical implementation. The verification has shown the expected monotonous convergence, which is indeed an important feature in the FEM. Even for the case of boundary conditions with a given surface charge, our proposed implementation has this feature such that a posteriori error analysis is possible for more "complex" problems without a closed-form solution.

Additionally, the charge density boundary condition has been verified by comparing with the equivalent potential boundary condition, which is a simple benchmark test for consistency. The two boundary conditions gave essentially the same results for electric field and potential. Therefore, we conclude that the use of continuous and discontinuous Lagrange elements is adequate for this problem.

Finally, we have applied the methodology for an industrial application by using an irreversible part for the charge potential and determined the quality factor of a capacitor and provide a transient solution that accounts for dielectric loss. Accurate computations are of importance for testing the predictive capacity of reduced order systems [44] as well to design sophisticated structures by using novel dielectric designs [45–47].

Acknowledgements Yiming Liu gratefully acknowledges financial support from the China Scholarship Council. The authors are also grateful to Dr.-Ing. Sebastian Glane and M.Sc. Wilhelm Rickert from Technische Universität Berlin, Institute of Mechanics, who provided insight and expertise that greatly assisted the research.

Open Access This article is licensed under a Creative Commons Attribution 4.0 International License, which permits use, sharing, adaptation, distribution and reproduction in any medium or format, as long as you give appropriate credit to the original author(s) and the source, provide a link to the Creative Commons licence, and indicate if changes were made. The images or other third party material in this article are included in the article's Creative Commons licence, unless indicated otherwise in a credit line to the material. If material is not included in the article's Creative Commons licence and your intended use is not permitted by statutory regulation or exceeds the permitted use, you will need to obtain permission directly from the copyright holder. To view a copy of this licence, visit http://creativecommons.org/licenses/by/4.0/.

Funding Open access funding provided by Uppsala University. Yiming Liu is funded by China Scholarship Council (CSC, 202006120055).

References

1. Nicholson, J.W.: II.-oblate spheroidal harmonics and their applications. Philos. Trans. Roy. Soc. Lond. Ser. A Contain. Pap. Math. Phys. Charact. **224**(616–625), 49–93 (1924)
2. Love, R.R.: The electrostatic field of two equal circular co-axial conducting disks. Q. J. Mech. Appl. Mech. **2**, 428–451 (1949)
3. Love, E.R.: The potential due to a circular parallel plate condenser. Mathematika **37**(2), 217–231 (1990)
4. Sneddon, I.N.: Mixed Boundary Value Problems in Potential Theory. North-Holland Publishing Company (1966)
5. Carlson, G., Illman, B.: The circular disk parallel plate capacitor. Am. J. Phys. **62**(12), 1099–1105 (1994)
6. Milovanović, G.V.: Integral equations of Love's type and applications. In: Zbornik radova Konferencije MIT 2013, Beograd, pp. 450–457 (2014)
7. Pastore, P.: The numerical treatment of Love's integral equation having very small parameter. J. Comput. Appl. Math. **236**(6), 1267–1281 (2011)
8. Panda, S., Martha, S.C., Chakrabarti, A.: A modified approach to numerical solution of Fredholm integral equations of the second kind. Appl. Math. Comput. **271**, 102–112 (2015)
9. Atkinson, W., Young, J.H., Brezovich, I.: An analytic solution for the potential due to a circular parallel plate capacitor. J. Phys. A Math. Gen. **16**(12), 2837 (1983)
10. Hughes, B.D.: Comment on the potential due to a circular parallel plate capacitor. J. Phys. A Math. Gen. **17**, 1385–1386 (1984)
11. Parker, G.: Electric field outside a parallel plate capacitor. Am. J. Phys. **70**(5), 502–507 (2002)
12. Paffuti, G., Cataldo, E., Di Lieto, A., Maccarrone, F.: Circular plate capacitor with different discs. Proc. Roy. Soc. A Math. Phys. Eng. Sci. **472**(2194), 20160574 (2016)
13. Kirchhoff, G.R.: Zur Theorie des Condensators, pp. 48–50 (1879)
14. Hutson, V.: The circular plate condenser at small separations. In: Mathematical Proceedings of the Cambridge Philosophical Society, vol. 59, pp. 211–224, Cambridge University Press (1963)
15. Wintle, H., Kurylowicz, S.: Edge corrections for strip and disc capacitors. IEEE Trans. Instrum. Meas. **1**, 41–47 (1985)
16. Norgren, M., Jonsson, B.L.G.: The capacitance of the circular parallel plate capacitor obtained by solving the Love integral equation using an analytic expansion of the kernel. arXiv preprint arXiv:0909.3674 (2009)
17. Milovanović, G.V., Joksimović, D.: Properties of Boubaker polynomials and an application to Love's integral equation. Appl. Math. Comput. **224**, 74–87 (2013)
18. Reichert, B., Ristivojevic, Z.: Analytical results for the capacitance of a circular plate capacitor. Phys. Rev. Res. **2**(1), 013289 (2020)
19. Xiang, Y.: The electrostatic capacitance of an inclined plate capacitor. J. Electrostat. **64**(1), 29–34 (2006)
20. Catalán Izquierdo, S., Bueno Barrachina, J.M., Cañas Peñuelas, C.S., Cavallé Sesé, F.: Capacitance evaluation on parallel-plate capacitors by means of finite element analysis. Renew. Energy Power Qual. J. **1**(7), 613–616 (2009)
21. Hong, W., Suo, Z., Zhang, Z.: Dynamics of terraces on a silicon surface due to the combined action of strain and electric current. J. Mech. Phys. Solids **56**(1), 267–278 (2008)
22. Mehnert, M., Hossain, M., Steinmann, P.: A complete thermo-electro-viscoelastic characterization of dielectric elastomers, part I: experimental investigations. J. Mech. Phys. Solids **157**, 104603 (2021)
23. Mehnert, M., Hossain, M., Steinmann, P.: A complete thermo-electro-viscoelastic characterization of dielectric elastomers, part ii: Continuum modeling approach. J. Mech. Phys. Solids **157**, 104625 (2021)
24. Sharma, A.K., Joglekar, M.: A computationally efficient locking free numerical framework for modeling visco-hyperelastic dielectric elastomers. Comput. Methods Appl. Mech. Eng. **352**, 625–653 (2019)
25. Schlögl, T., Leyendecker, S.: Electrostatic-viscoelastic finite element model of dielectric actuators. Comput. Methods Appl. Mech. Eng. **299**, 421–439 (2016)
26. Zäh, D., Miehe, C.: Multiplicative electro-elasticity of electroactive polymers accounting for micromechanically-based network models. Comput. Methods Appl. Mech. Eng. **286**, 394–421 (2015)
27. Cai, Z., Wang, X., Luo, B., Hong, W., Wu, L., Li, L.: Multiscale design of high-voltage multilayer energy-storage ceramic capacitors. J. Am. Ceram. Soc. **101**(4), 1607–1615 (2018)
28. Chen, H., Mukherjee, S., Aluru, N.: Charge distribution on thin semiconducting silicon nanowires. Comput. Methods Appl. Mech. Eng. **197**(41–42), 3366–3377 (2008)
29. Kovetz, A.: Electromagnetic Theory, vol. 975. Oxford University Press (2000)
30. Monk, P., et al.: Finite Element Methods for Maxwell's EWquations. Oxford University Press (2003)

31. Fleisch, D.: A Student's Guide to Maxwell's Equations. Cambridge University Press (2008)
32. Müller, W.H.: An Expedition to Continuum Theory. Springer (2014)
33. Abali, B.E., Reich, F.A.: Thermodynamically consistent derivation and computation of electro-thermo-mechanical systems for solid bodies. Comput. Methods Appl. Mech. Eng. **319**, 567–595 (2017)
34. Abali, B.E., Queiruga, A.F.: Theory and computation of electromagnetic fields and thermomechanical structure interaction for systems undergoing large deformations. J. Comput. Phys. **394**, 200–231 (2019)
35. Abali, B.E.: Computational Reality. Advanced Structured Materials, vol. 55. Springer Nature, Singapore (2017)
36. Zohdi, T.I.: Finite Element Primer for Beginners. Springer (2018)
37. Arnold, D.N., Falk, R.S., Winther, R.: Finite element exterior calculus, homological techniques, and applications. Acta Numer. **15**, 1–155 (2006)
38. Zohdi, T.I., Abali, B.E.: Modeling of power transmission and stress grading for corona protection. Comput. Mech. **62**(3), 411–420 (2018)
39. Abali, B.E., Zohdi, T.I.: Multiphysics computation of thermal tissue damage as a consequence of electric power absorption. Comput. Mech. **65**(1), 149–158 (2020)
40. Chen, Q., Konrad, A.: A review of finite element open boundary techniques for static and quasi-static electromagnetic field problems. IEEE Trans. Magn. **33**, 663–676 (1997)
41. Weir, W.B.: Automatic measurement of complex dielectric constant and permeability at microwave frequencies. Proc. IEEE **62**(1), 33–36 (1974)
42. Nasedkin, A.V., Eremeyev, V.A.: Spectral Properties of Piezoelectric Bodies with Surface Effects, pp. 105–121. Springer, Berlin (2013)
43. Nasedkin, A.V., Eremeyev, V.A.: Harmonic vibrations of nanosized piezoelectric bodies with surface effects. ZAMM J. Appl. Math. Mech. Zeitschrift für Angewandte Mathematik und Mechanik **94**(10), 878–892 (2014)
44. Abali, B.E., Zohdi, T.I.: On the accuracy of reduced-order integrated circuit simulators for computing the heat production on electronic components. J. Comput. Electron. **17**(2), 625–636 (2018)
45. Cao, X., Zhang, M., Zhang, Z., Xu, Y., Xiao, Y., Li, T.: Review of soft linear actuator and the design of a dielectric elastomer linear actuator. Acta Mech. Solida Sin. **32**(5), 566–579 (2019)
46. Hajiesmaili, E., Khare, E., Chortos, A., Lewis, J., Clarke, D.R.: Voltage-controlled morphing of dielectric elastomer circular sheets into conical surfaces. Extreme Mech. Lett. **30**, 100504 (2019)
47. Croce, S., Neu, J., Moretti, G., Hubertus, J., Schultes, G., Rizzello, G.: Finite element modeling and validation of a soft array of spatially coupled dielectric elastomer transducers. Smart Mater. Struct. **31**(8), 084001 (2022)

Publisher's Note Springer Nature remains neutral with regard to jurisdictional claims in published maps and institutional affiliations.